A new type of modified WENO schemes for solving hyperbolic conservation laws[1]

Jun Zhu[2] and Jianxian Qiu[3]

Abstract

In this paper we design a new type of the third order and fifth order modified weighted essentially non-oscillatory (MWENO) schemes in the finite difference framework for solving the hyperbolic conservation laws. These schemes adapt between the linear upwind scheme and the WENO scheme automatically by the usage of a new simple switching principle. The methodology to reconstruct numerical fluxes for the MWENO schemes is split into two parts: if all extreme points of the reconstruction polynomial for numerical flux in the big spatial stencil are located outside of the stencil, the the numerical flux is approximated directly by the reconstruction polynomial, and the approximation is a linear and high order accuracy; otherwise the WENO procedure in [12, 18] is applied to reconstruct the numerical flux. The main advantage of these new MWENO schemes is their robustness and efficiency comparing with the classical WENO schemes specified in [12, 18]. The MWENO schemes can be applied to compute some extreme test cases such as the Sedov blast wave, the Leblanc and the high Mach number astrophysical jet problems et al. by using a normal CFL number without any further positivity preserving procedure for the purpose of controlling the concurrence of the negative density and pressure. Extensive numerical results are provided to illustrate the good performance of the MWENO schemes.

Key Words: WENO scheme, hyperbolic conservation laws, finite difference framework.

AMS(MOS) subject classification: 65M60, 35L65

[1]The research is partly supported by NSFC grants 11372005, 11571290 and 91530107.

[2]College of Science, Nanjing University of Aeronautics and Astronautics, Nanjing, Jiangsu 210016, P.R. China. E-mail: zhujun@nuaa.edu.cn.

[3]School of Mathematical Sciences and Fujian Provincial Key Laboratory of Mathematical Modeling and High-Performance Scientific Computing, Xiamen University, Xiamen, Fujian 361005, P.R. China. E-mail: jxqiu@xmu.edu.cn.

1 Introduction

In this paper we present a new type of modified weighted essentially non-oscillatory (MWENO) schemes in the finite difference framework, which can be applied to compute the rather extreme test cases such as the Sedov blast wave problem, the Leblanc problem and the high Mach number astrophysical jet problem et al. directly with normal CFL number and without any additional positivity preserving procedure. For the sake of devising robust, accurate and efficient methods for numerically solving these problems is of considerable importance and as expected, has attracted the interest of many researchers and practitioners. In recent decades, many high order numerical methods have been developed to solve these problems. Among them, we would like to mention essentially non-oscillatory (ENO) and weighted ENO (WENO) schemes, which have been applied quite successfully to solve the problems with shocks, contact discontinuities and sophisticated smooth structures. In order to achieve uniform high order accuracy in smooth region, Harten and Osher [10] gave a weaker version of the total variation diminishing (TVD) criterion [7] and on which they established a basis for the reconstruction of high order ENO type schemes. Then ENO schemes were developed by Harten et al. [9] to solve one dimensional problems. The most important thought of ENO schemes is to apply the most smooth stencil among all candidate stencils to approximate the variables at cell boundaries for the purpose of obtaining high order accuracy in smooth region and avoiding spurious oscillations nearby discontinuities simultaneously. We can also find this thought in [19, 20]. In 1994, the first high order accurate WENO scheme was introduced by Liu, Osher and Chan [16], in which instead of using just one optimal smooth candidate stencil, a linear combination of all candidate stencils including nonsmooth stencils is used. In 1996, third and fifth order finite difference WENO schemes in multi-space dimensions were constructed by Jiang and Shu [12], with a general framework for the designing of new smoothness indicators and nonlinear weights. A key idea in WENO schemes is a linear combination of lower order numerical fluxes or reconstruction to obtain a higher order approximation. For the system case, the WENO

schemes are based on local characteristic decomposition and numerical flux splitting method to avoid nonphysical oscillations nearby strong shocks or contact discontinuities.

The finite difference and finite volume schemes of ENO and WENO [1, 2, 8, 11, 12, 16, 19, 20, 26] are quite successful in numerical simulations for problems with strong discontinuities and sophisticated smooth structures. But for some extreme test cases, the additional positivity preserving procedure or/and reduced CFL number are needed to control the concurrence of negative density and negative pressure. A series of high order positivity preserving procedure have been developed for finite volume and finite difference high order methods [13, 21, 22, 23, 24, 25]. Though the WENO schemes with the additional positivity preserving procedure can work well for the rather extreme test cases, the computational efficiency is reduced due to the additional procedure and/or reduced CFL number. In this paper, we present the third order and fifth order MWENO schemes in the finite difference framework for solving the hyperbolic conservation laws in one and two dimensions. Comparing with the classical WENO schemes [12, 18], MWENO schemes are more robust and efficient with less numerical errors in smooth region. And these schemes can be applied to compute some benchmark extreme cases including the Sedov blast wave, the Leblanc and the high Mach number astrophysical jet problems et al. directly using normal CFL number without any additional positivity preserving procedure. The main procedures of MWENO schemes are narrated in the following. First, in the finite difference framework, a polynomial based on the nodal point information of the numerical flux is reconstructed in the interval of the big spatial stencil. Second, the location of the extreme points of the reconstructed polynomial is identified. Third, if the extreme points of the reconstruction polynomial in the big spatial stencil are located outside of the same stencil, the reconstructed polynomial is adapted to approximate the numerical flux straightforward, the approximation is of high order accuracy and a linear upwind scheme with less numerical errors is obtained; otherwise the WENO reconstruction procedure [12, 18] is applied to reconstruct the numerical flux and a WENO scheme is applicable. For the system case, WENO reconstruction is based on local charac-

teristic decompositions and flux splitting to avoid spurious oscillations, and the cost of the computation of smoothness indicators, nonlinear weights and local characteristic decompositions is very high. The new MWENO schemes designed in this paper are a hybrid of WENO with an optimal linear combination of lower order of reconstructions. For the linear upwind reconstructions we can avoid the performance of the local characteristic decompositions and the computation of the nonlinear weights et al., hence reducing the cost but still maintaining non-oscillatory properties for the problems with strong shocks including some extreme test cases without any further special methodologies.

The organization of the paper is as follows: in Section 2, we construct and analyze the finite difference modified WENO schemes in detail. In Section 3, some benchmark numerical tests including low density (vacuum), low pressure with strong shocks are presented to verify the numerical accuracy, efficiency and robustness of the new MWENO schemes. Concluding remarks are given in Section 4.

2 Modified WENO scheme

In this section, we first consider one dimensional hyperbolic conservation laws

$$\begin{cases} u_t + f_x(u) = 0, \\ u(x,0) = u_0(x). \end{cases} \tag{2.1}$$

The semidiscretization formula is written as

$$\frac{du}{dt} = L(u), \tag{2.2}$$

where $L(u)$ is the high order spatial discrete formulation of $-f_x(u)$. The uniform mesh is distributed into cells $I_i = [x_{i-1/2}, x_{i+1/2}]$, with the cell size $x_{i+1/2} - x_{i-1/2} = h$ and cell centers $x_i = \frac{1}{2}(x_{i+1/2} + x_{i-1/2})$. $u_i(t)$ is defined as $u(x_i, t)$. Herein, the right hand side of (2.2) can be written as

$$L(u_i(t)) = -\frac{1}{h}(\hat{f}_{i+1/2} - \hat{f}_{i-1/2}), \tag{2.3}$$

where $\hat{f}_{i+1/2}$ is a numerical flux which is a high order approximation of flux $f(u)$ at the boundary $x_{i+1/2}$ of target cell I_i. If the numerical flux $\hat{f}_{i+1/2}$ is taken to be the (2r+1)th order approximation to $v_{i+1/2} = v(x_{i+1/2})$, where $v(x)$ is defined as

$$f(u(x)) = \frac{1}{h}\int_{x-h/2}^{x+h/2} v(\eta)d\eta, \tag{2.4}$$

then $\frac{1}{h}(\hat{f}_{i+1/2} - \hat{f}_{i-1/2})$ is the (2r+1)th order approximation to $f_x(u)$ at $x = x_i$. For the purpose of keeping the stability, we need consider the upwind quality of the schemes. We will split flux $f(u)$ into two parts: $f(u) = f^+(u) + f^-(u)$ with $\frac{df^+(u)}{du} \geq 0$ and $\frac{df^-(u)}{du} \leq 0$. Here, a simplest Lax-Friedrichs splitting is applied as

$$f^{\pm}(u) = \frac{1}{2}(f(u) \pm \alpha u), \tag{2.5}$$

in which α is set as $\max_u |f'(u)|$ over the whole range of u. Let $\hat{f}^+_{i+\frac{1}{2}}$ and $\hat{f}^-_{i+\frac{1}{2}}$ be the numerical fluxes at $x_{i+1/2}$ which are $(2r+1)$th order approximation of $v(x)$ in (2.4) with the positive and negative parts of $f(u)$, respectively, and $\hat{f}_{i+1/2}$ is defined as $\hat{f}^+_{i+\frac{1}{2}} + \hat{f}^-_{i+\frac{1}{2}}$.

Now we describe in detail for the reconstruction procedure of $\hat{f}^+_{i+\frac{1}{2}}$, and the reconstruction procedure of $\hat{f}^-_{i+\frac{1}{2}}$ is mirror symmetric with respect to $x_{i+1/2}$ of that for $\hat{f}^+_{i+\frac{1}{2}}$. From the definition of $v(x)$ in (2.4) for $f^+(u)$, we have

$$f^+(u_i) = \frac{1}{h}\int_{x_{i-1/2}}^{x_{i+1/2}} v(\eta)d\eta = v_i, \tag{2.6}$$

where v_i is the cell average of $v(x)$ on the I_i.

Step 1. Choose the following big stencil: $T = \{I_{i-r}, ..., I_{i+r}\}$. It is easy to obtain the reconstructed polynomial which based on the nodal point numerical flux satisfying

$$\frac{1}{h}\int_{I_j} p(\eta)d\eta \;=\; \frac{1}{h}\int_{I_j} v(\eta)d\eta = v_j = f^+(u_j),\ j = i-r, ..., i+r. \tag{2.7}$$

Let $\xi = \frac{(x-x_i)}{h}$, for example, when $r = 1$, we have:

$$p(x) \;=\; -\frac{1}{24}[(v_{i-1} - 26v_i + v_{i+1}) + 12(v_{i-1} - v_{i+1})\xi - 12(v_{i-1} - 2v_i + v_{i+1})\xi^2], \tag{2.8}$$

and its first derivative polynomial is

$$p'(x) \;=\; \frac{1}{2h}[-v_{i-1} + v_{i+1} + 2(v_{i-1} - 2v_i + v_{i+1})\xi]. \tag{2.9}$$

When $r = 2$:

$$\begin{aligned} p(x) &= \frac{1}{1920}[(-116v_{i-1} + 9v_{i-2} + 2134v_i - 116v_{i+1} + 9v_{i+2}) - 40(34v_{i-1} - \\ &\quad 5v_{i-2} - 34v_{i+1} + 5v_{i+2})\xi + 120(12v_{i-1} - v_{i-2} - 22v_i + 12v_{i+1} - \\ &\quad v_{i+2})\xi^2 + 160(2v_{i-1} - v_{i-2} - 2v_{i+1} + v_{i+2})\xi^3 - 80(4v_{i-1} - v_{i-2} - \\ &\quad 6v_i + 4v_{i+1} - v_{i+2})\xi^4)], \end{aligned} \tag{2.10}$$

and its first derivative polynomial is

$$\begin{aligned} p'(x) &= \frac{1}{48h}[(-34v_{i-1} + 5v_{i-2} + 34v_{i+1} - 5v_{i+2}) + 6(12v_{i-1} - v_{i-2} - 22v_i + \\ &\quad 12v_{i+1} - v_{i+2})\xi + 12(2v_{i-1} - v_{i-2} - 2v_{i+1} + v_{i+2})\xi^2 + 8(-4v_{i-1} + \\ &\quad v_{i-2} + 6v_i - 4v_{i+1} + v_{i+2})\xi^3)]. \end{aligned} \tag{2.11}$$

Step 2. Identify the extreme points of the reconstruction polynomial $p(x)$. First, we compute the zero points of $p'(x)$, if $p'(x)$ has real zero points, then it is easy to identify whether these real zero points are extreme points of $p(x)$ or not. When $r = 1$, the degree of $p'(x)$ is at most one, then there is at most one real zero point, and real zero point is the extreme point of $p(x)$. When $r = 2$, the degree of $p'(x)$ is at most three, and we can solve the real zero points of $p'(x)$ explicitly [3], and one is the extreme point of $p(x)$ if it is not doubled zero point of $p'(x)$.

Step 3. If there is not the extreme point of the reconstruction polynomial $p(x)$, or all extreme points are located outside of the big spatial stencil T, the final reconstruction of the numerical flux of $f^+(u)$ at $x = x_{i+1/2}$ is directly given by $\hat{f}^+_{i+1/2} = p(x_{i+\frac{1}{2}})$, and which is a linear upwind approximation to $f^+(u)$. Then the procedure jumps to Step 5.

Step 4. If there are the extreme points of the reconstruction polynomial $p(x)$ which are located in the big spatial stencil T, then the following WENO procedure is fulfilled to reconstruct the $\hat{f}^+_{i+1/2}$. The stencil T is divided into $r+1$ smaller stencils: $S_0 = \{I_{i-r}, ..., I_i\}$, ..., $S_r = \{I_i, ..., I_{i+r}\}$. Similarly as specified in Step 1, the polynomials $p_l(x)$, $l = 0, ..., r$ are

constructed in the associated smaller stencils to approximate the function $v(x)$ with

$$\frac{1}{h}\int_{I_j} p_l(\eta)d\eta = \frac{1}{h}\int_{I_j} v(\eta)d\eta = v_j = f^+(u_j),\ j = i-r+l, ..., i+l,\ l = 0, ..., r.$$

The values of the functions $p_l(x)$ at the point $x_{i+1/2}$ of cell I_i, can be written as a linear combination of $\{v_j\}$ (see [12, 18]). Then the linear weights are calculated on condition that $p(x_{i+1/2}) = \sum_{l=0}^{r} \gamma_l p_l(x_{i+1/2})$. For the smaller stencils S_l, we compute the smoothness indicators β_l, which measure how smooth the functions $p_l(x)$ are in the target cell I_i. The smaller these smoothness indicators, the smoother the functions are in the target interval. We use the same recipe for the smoothness indicators as in [12, 18]

$$\beta_l = \sum_{\alpha=1}^{r}\int_{I_i} h^{2\alpha-1}(\frac{d^\alpha p_l(x)}{dx^\alpha})^2 dx, \tag{2.12}$$

Then the nonlinear weights based on the linear weights and associated smoothness indicators [12, 18] are

$$\omega_l = \frac{\overline{\omega}_l}{\sum_{k=0}^{r}\overline{\omega}_k},\ \ \overline{\omega}_l = \frac{\gamma_l}{(\varepsilon+\beta_l)^2}. \tag{2.13}$$

Where γ_l are the linear weights, for $r=1$, $\gamma_0 = \frac{1}{3}, \gamma_1 = \frac{2}{3}$, for $r=2$, $\gamma_0 = \frac{1}{10}, \gamma_1 = \frac{3}{5}, \gamma_2 = \frac{3}{10}$, respectively, and ε is a small positive number to avoid division by zero, ε is set as 10^{-6} in the paper. The final reconstruction of the numerical flux $f(u)$ at $x = x_{i+1/2}$ is given by

$$\hat{f}^+_{i+1/2} = \sum_{l=0}^{r}\omega_l p_l(x_{i+\frac{1}{2}}).$$

Step 5. The semidiscrete scheme (2.2) is discretized in time by Runge-Kutta method, such as a fourth order one [19]

$$\begin{cases} u^{(1)} &= u^n + \frac{1}{2}\Delta t L(u^n), \\ u^{(2)} &= u^n + \frac{1}{2}\Delta t L(u^{(1)}), \\ u^{(3)} &= u^n + \Delta t L(u^{(2)}), \\ u^{n+1} &= -\frac{1}{3}u^n + \frac{1}{3}u^{(1)} + \frac{2}{3}u^{(2)} + \frac{1}{3}u^{(3)} + \frac{1}{6}\Delta t L(u^{(3)}). \end{cases} \tag{2.14}$$

Remarks: For system cases, such as the compressible Euler equations, we first split the flux f into two parts $f = f^+ + f^-$, such that the eigenvalues of Jacobian matrixes $\frac{df^+}{du}$ and $\frac{df^-}{du}$ are positive and negative, respectively. Then, we reconstruct the polynomials on the

big spatial stencil T for all components of f^+, respectively. If the extreme points of all the reconstructed polynomials are located outside of T, the numerical fluxes of f^+ at $x = x_{i+1/2}$ are directly approximated by the values of the reconstructed polynomials at $x = x_{i+1/2}$, and the approximations are linear and the local characteristic projection is avoided to save the computational cost. Otherwise, all of the reconstructions are performed in the local characteristic directions, for each local characteristic direction we follow Step 1 to Step 4 to reconstruct the numerical fluxes for f^+ at $x = x_{i+1/2}$. The reconstruction procedure of the numerical fluxes for f^- at $x = x_{i+1/2}$ is mirror symmetric with respect to $x_{i+1/2}$ of that for f^+ at $x = x_{i+1/2}$. When the methods are extended from one to two dimensional cases, the reconstruction procedure is performed in a "dimension-by-dimension" manner.

3 Numerical tests

In this section we present the results of numerical tests of the third and fifth order MWENO schemes which are described in the previous section comparing with the classical WENO schemes [12, 18]. The CFL number is set as usual as 0.6 for different WENO and MWENO schemes. WENO3, WENO5, MWENO3 and MWENO5 are denoted as the third order WENO, fifth order WENO, third order MWENO and fifth order MWENO schemes, respectively.

Example 3.1.

$$\frac{\partial}{\partial t}\begin{pmatrix}\rho\\ \rho\mu\\ E\end{pmatrix}+\frac{\partial}{\partial x}\begin{pmatrix}\rho\mu\\ \rho\mu^2+p\\ \mu(E+p)\end{pmatrix}=0. \tag{3.1}$$

In which ρ is density, μ is the velocity in x direction, E is total energy and p is pressure. The initial conditions are: (1) $\rho(x,0) = 1 + 0.99\sin(x)$; (2) $\rho(x,0) = 1 + 0.999\sin(x)$; (3) $\rho(x,0) = 1 + 0.99999\sin(x)$; and $\mu(x,0) = 1$, $p(x,0) = 1$, $\gamma = 1.4$. The computing domain is $x \in [0, 2\pi]$. Periodic boundary condition is applied in this test. The exact solutions are: (1) $\rho(x,t) = 1+0.99\sin(x-t)$; (2) $\rho(x,t) = 1+0.999\sin(x-t)$; (3) $\rho(x,t) = 1+0.99999\sin(x-t)$, respectively. The final time is $T = 0.1$. The WENO schemes [12] do not work for the case (3)

Table 3.1: 1D-Euler equations: initial data $\rho(x,0) = 1+0.99\sin(x)$, $\mu(x,0) = 1$ and $p(x,0) = 1$. MWENO scheme and WENO scheme. $T = 0.1$. L^1 and L^∞ errors.

	MWENO3 scheme				WENO3 scheme			
grid points	L^1 error	order	L^∞ error	order	L^1 error	order	L^∞ error	order
40	4.38E-3		1.96E-2		5.63E-3		2.27E-2	
80	1.30E-3	1.74	8.30E-3	1.25	1.65E-3	1.77	9.50E-3	1.26
160	1.79E-4	2.87	2.12E-3	1.97	3.34E-4	2.31	3.02E-3	1.65
320	3.64E-6	5.61	1.02E-4	4.37	3.35E-5	3.31	4.31E-4	2.81
640	8.92E-8	5.35	2.04E-6	5.64	2.02E-6	4.04	2.07E-5	4.38
1280	7.97E-9	3.48	5.05E-8	5.33	1.17E-7	4.10	6.73E-7	4.94
	MWENO5 scheme				WENO5 scheme			
grid points	L^1 error	order	L^∞ error	order	L^1 error	order	L^∞ error	order
40	1.47E-6		6.39E-6		8.58E-6		1.74E-5	
80	3.94E-8	5.22	1.29E-7	5.62	2.77E-7	4.95	5.68E-7	4.93
160	1.24E-9	4.98	3.45E-9	5.22	8.74E-9	4.98	1.78E-8	4.99
320	3.92E-11	4.99	8.90E-11	5.27	2.74E-10	4.99	5.45E-10	5.02
640	1.22E-12	4.99	1.93E-12	5.52	8.59E-12	4.99	1.63E-11	5.06
1280	3.83E-14	4.99	6.59E-14	4.87	2.68E-13	4.99	4.70E-13	5.11

for the computed density appears negative. The numerical errors and orders of the density for the MWENO schemes and the WENO schemes [12] are shown in Table 3.1 and Table 3.2, we can see that both the MWENO and WENO achieve the designed order, and numerical errors of the MWENO are smaller than those of the WENO at the same meshes. In Table 3.3, we show The numerical errors and orders of the density for the MWENO schemes, we also can see that the MWENO3 and MWENO5 schemes achieve their optimal order without breaking down during the simulations. In Figure 3.1 and Figure 3.2 we show numerical errors against CPU times for the MWENO schemes and WENO schemes for case (1) and (2). We can see that the MWENO schemes use less CPU times and have smaller numerical errors than those for the WENO schemes at the same meshes. The MWENO schemes are more efficient and robust than the WENO schemes in this one dimensional benchmark test case with different initial conditions.

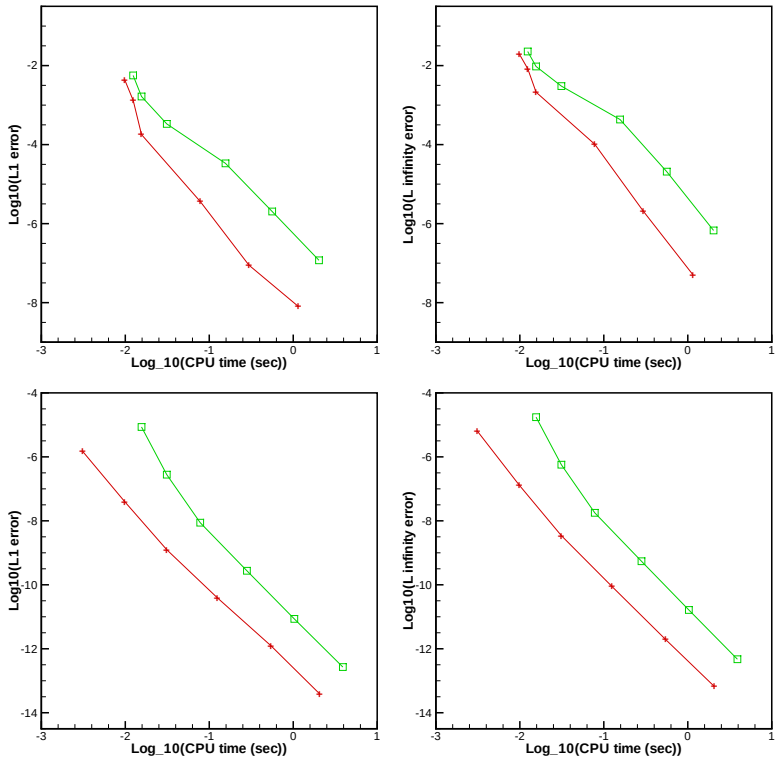

Figure 3.1: 1D-Euler equations: initial data $\rho(x,0) = 1 + 0.99\sin(x)$, $\mu(x,0) = 1$ and $p(x,0) = 1$. Computing time and error. Plus signs and a solid line denote the results of the MWENO schemes; squares and a solid line denote the results of the WENO schemes. From top to bottom: the third order scheme; the fifth order scheme.

Table 3.2: 1D-Euler equations: initial data $\rho(x,0) = 1 + 0.999\sin(x)$, $\mu(x,0) = 1$ and $p(x,0) = 1$. MWENO scheme and WENO scheme. $T = 0.1$. L^1 and L^∞ errors.

	MWENO3 scheme				WENO3 scheme			
grid points	L^1 error	order	L^∞ error	order	L^1 error	order	L^∞ error	order
40	6.04E-3		2.38E-2		6.97E-3		2.64E-2	
80	1.88E-3	1.68	1.09E-2	1.13	2.30E-3	1.60	1.22E-2	1.11
160	3.84E-4	2.30	3.75E-3	1.54	6.50E-4	1.82	5.10E-3	1.27
320	3.79E-5	3.34	7.87E-4	2.25	1.36E-4	2.25	1.62E-3	1.65
640	7.04E-7	5.75	2.51E-5	4.96	1.73E-5	2.98	2.92E-4	2.47
1280	2.79E-8	4.65	5.42E-7	5.53	1.16E-6	3.88	1.71E-5	4.09
	MWENO5 scheme				WENO5 scheme			
grid points	L^1 error	order	L^∞ error	order	L^1 error	order	L^∞ error	order
40	2.83E-6		1.08E-5		1.93E-5		3.83E-5	
80	1.10E-7	4.68	2.60E-7	5.38	7.74E-7	4.63	1.54E-6	4.63
160	3.66E-9	4.91	8.15E-9	4.99	2.57E-8	4.91	5.02E-8	4.94
320	1.17E-10	4.96	2.28E-10	5.15	8.23E-10	4.96	1.58E-9	4.98
640	3.70E-12	4.98	6.99E-12	5.03	2.59E-11	4.99	4.88E-11	5.02
1280	1.16E-13	4.99	2.03E-13	5.10	8.11E-13	4.99	1.50E-12	5.02

Table 3.3: 1D-Euler equations: initial data $\rho(x,0) = 1 + 0.99999\sin(x)$, $\mu(x,0) = 1$ and $p(x,0) = 1$. MWENO scheme. $T = 0.1$. L^1 and L^∞ errors.

	MWENO3 scheme				MWENO5 scheme			
grid points	L^1 error	order	L^∞ error	order	L^1 error	order	L^∞ error	order
40	6.34E-3		2.46E-2		6.56E-6		1.83E-5	
80	1.98E-3	1.68	1.13E-2	1.12	4.20E-7	3.96	8.61E-7	4.41
160	4.33E-4	2.19	4.11E-3	1.47	1.82E-8	4.52	3.44E-8	4.64
320	6.48E-5	2.74	1.14E-3	1.84	8.13E-10	4.48	1.45E-9	4.56
640	5.76E-6	3.48	1.86E-4	2.62	3.14E-11	4.69	5.51E-11	4.72
1280	5.47E-7	3.39	2.19E-5	3.08	1.08E-12	4.85	1.87E-12	4.87

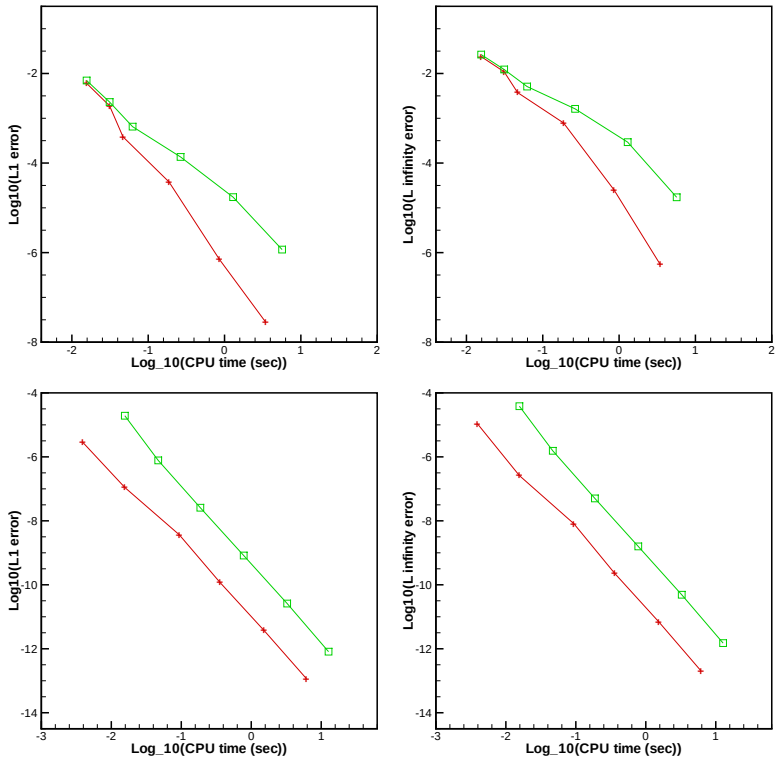

Figure 3.2: 1D-Euler equations: initial data $\rho(x,0) = 1 + 0.999\sin(x)$, $\mu(x,0) = 1$ and $p(x,0) = 1$. Computing time and error. Plus signs and a solid line denote the results of the MWENO scheme; squares and a solid line denote the results of the WENO scheme. From top to bottom: the third order scheme; the fifth order scheme.

Example 3.2.

$$\frac{\partial}{\partial t}\begin{pmatrix}\rho\\ \rho\mu\\ \rho\nu\\ E\end{pmatrix}+\frac{\partial}{\partial x}\begin{pmatrix}\rho\mu\\ \rho\mu^2+p\\ \rho\mu\nu\\ \mu(E+p)\end{pmatrix}+\frac{\partial}{\partial y}\begin{pmatrix}\rho\nu\\ \rho\mu\nu\\ \rho\nu^2+p\\ \nu(E+p)\end{pmatrix}=0. \tag{3.2}$$

In which ρ is density; μ and ν are the velocities in the x and y directions, respectively; E is total energy; and p is pressure. The initial conditions are: (1) $\rho(x,y,0)=1+0.99\sin(x+y)$; (2) $\rho(x,y,0)=1+0.999\sin(x+y)$; (3) $\rho(x,y,0)=1+0.99999\sin(x+y)$; and $\mu(x,y,0)=1$, $\nu(x,y,0)=1$, $p(x,y,0)=1$ and $\gamma=1.4$. The computing domain is $(x,y)\in[0,2\pi]\times[0,2\pi]$. Periodic boundary conditions are applied in both directions. We compute the solution up to $T=0.1$. As in Example 3.1, the WENO schemes also do not work for the case (3) for the computed density appears negative. The numerical errors and orders of the density for the MWENO schemes and the WENO schemes are shown in Table 3.4 and Table 3.5, we can see that both the MWENO and WENO schemes achieve their designed order of accuracy, and numerical errors of the MWENO3 and MWENO5 schemes are smaller than those of the WENO3 and WENO5 schemes at the same meshes. In Table 3.6, we can only show The numerical errors and orders of the density for the MWENO3 and MWENO5 schemes, we also can see that the MWENO schemes achieve their optimal order accurately. In Figure 3.3 and Figure 3.4 we show numerical errors against CPU times for the MWENO schemes and WENO schemes for case (1) and case (2). We can see that the MWENO schemes use less CPU times and have smaller numerical errors in comparison with the WENO schemes at the same meshes. So the specified MWENO schemes are more efficient and robust than the classical WENO schemes in this two dimensional test case with three extreme density initial conditions.

Example 3.3. We solve the 1D Euler equations with Riemann initial condition for the Lax problem:

$$(\rho,u,p,\gamma)^T=\begin{cases}(0.445,0.698,3.528,1.4)^T, & x\in[-0.5,0),\\ (0.5,0,0.571,1.4)^T, & x\in[0,0.5].\end{cases} \tag{3.3}$$

For $T=0.16$, we present the exact solution and the computed density ρ obtained with the MWENO schemes comparing to the WENO schemes by using 200 grid points in Figure 3.5.

Table 3.4: 2D-Euler equations: initial data $\rho(x,y,0) = 1 + 0.99\sin(x+y)$, $\mu(x,y,0) = 1$, $\nu(x,y,0) = 1$ and $p(x,y,0) = 1$. MWENO scheme and WENO scheme. $T = 0.1$. L^1 and L^∞ errors.

	MWENO3 scheme				WENO3 scheme			
grid points	L^1 error	order	L^∞ error	order	L^1 error	order	L^∞ error	order
40× 40	7.02E-3		2.78E-2		8.92E-3		3.05E-2	
80× 80	1.88E-3	1.90	1.09E-2	1.35	2.71E-3	1.72	1.32E-2	1.20
160×160	2.93E-4	2.68	3.98E-3	1.46	6.07E-4	2.16	4.31E-3	1.62
320×320	5.16E-6	5.82	1.06E-4	5.22	6.42E-5	3.24	6.89E-4	2.64
640×640	1.50E-7	5.10	2.18E-6	5.60	3.86E-6	4.05	3.99E-4	4.10
	MWENO5 scheme				WENO5 scheme			
grid points	L^1 error	order	L^∞ error	order	L^1 error	order	L^∞ error	order
40× 40	2.32E-6		9.02E-6		1.63E-5		3.64E-5	
80× 80	7.37E-8	4.98	2.07E-7	5.44	5.17E-7	4.97	1.28E-6	4.82
160×160	2.33E-9	4.98	5.91E-9	5.13	1.63E-8	4.98	3.94E-8	5.03
320×320	7.30E-11	4.99	1.56E-10	5.24	5.11E-10	4.99	1.14E-9	5.10
640×640	2.28E-12	4.99	5.90E-12	4.72	1.60E-11	4.99	3.44E-11	5.05

Table 3.5: 2D-Euler equations: initial data $\rho(x,y,0) = 1 + 0.999\sin(x+y)$, $\mu(x,y,0) = 1$, $\nu(x,y,0) = 1$ and $p(x,y,0) = 1$. MWENO scheme and WENO scheme. $T = 0.1$. L^1 and L^∞ errors.

	MWENO3 scheme				WENO3 scheme			
grid points	L^1 error	order	L^∞ error	order	L^1 error	order	L^∞ error	order
40× 40	1.08E-2		3.52E-2		1.08E-2		3.58E-2	
80× 80	3.14E-3	1.79	1.58E-2	1.16	3.75E-3	1.52	1.67E-2	1.10
160×160	5.71E-4	2.46	5.09E-3	1.63	1.18E-3	1.66	7.97E-3	1.07
320×320	5.98E-5	3.25	1.06E-3	2.26	2.96E-4	2.01	2.92E-3	1.45
640×640	1.30E-6	5.51	3.73E-5	4.82	4.31E-5	2.78	5.21E-4	2.49
	MWENO5 scheme				WENO5 scheme			
grid points	L^1 error	order	L^∞ error	order	L^1 error	order	L^∞ error	order
40× 40	6.75E-6		1.68E-5		4.44E-5		9.68E-5	
80× 80	2.41E-7	4.80	5.20E-7	5.01	1.59E-6	4.79	4.01E-6	4.59
160×160	8.12E-9	4.89	1.56E-8	5.05	5.39E-8	4.88	1.30E-7	4.94
320×320	2.59E-10	4.96	4.79E-10	5.02	1.72E-9	4.96	3.91E-9	5.05
640×640	8.15E-12	4.99	1.50E-11	4.99	5.42E-11	4.99	1.30E-10	4.90

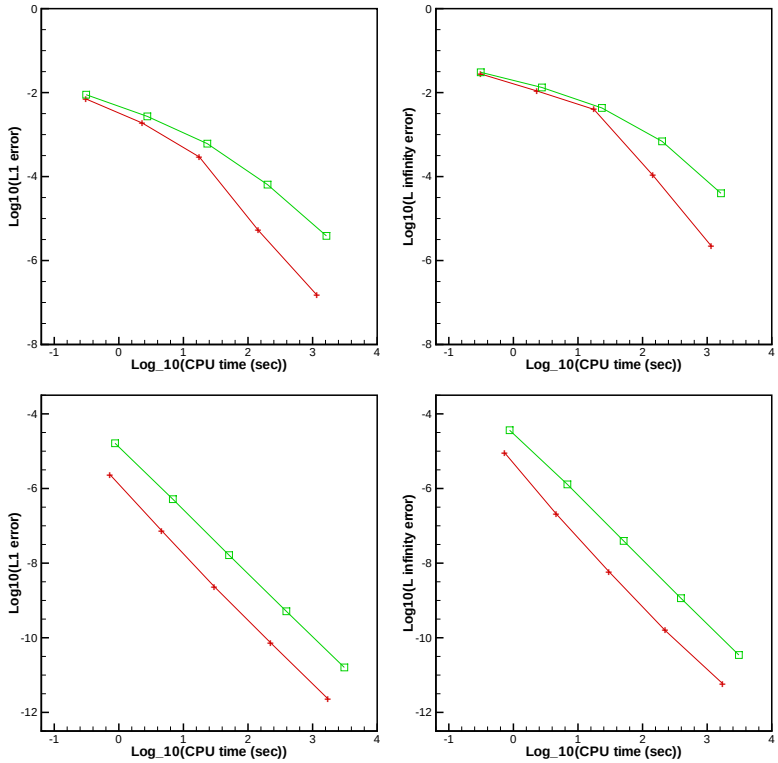

Figure 3.3: 2D-Euler equations: initial data $\rho(x,y,0) = 1 + 0.99\sin(x+y)$, $\mu(x,y,0) = 1$, $\nu(x,y,0) = 1$ and $p(x,y,0) = 1$. Computing time and error. Plus signs and a solid line denote the results of the MWENO scheme; squares and a solid line denote the results of the WENO scheme. From top to bottom: the third order scheme; the fifth order scheme.

Table 3.6: 2D-Euler equations: initial data $\rho(x,y,0) = 1 + 0.99999\sin(x+y)$, $\mu(x,y,0) = 1$, $\nu(x,y,0) = 1$ and $p(x,y,0) = 1$. MWENO scheme. $T = 0.1$. L^1 and L^∞ errors.

	MWENO3 scheme				MWENO5 scheme			
grid points	L^1 error	order	L^∞ error	order	L^1 error	order	L^∞ error	order
40× 40	1.11E-2		3.59E-2		1.69E-5		3.70E-5	
80× 80	3.26E-3	1.77	1.62E-2	1.15	8.39E-7	4.33	1.63E-6	4.50
160×160	6.28E-4	2.38	5.45E-3	1.57	4.13E-8	4.34	7.41E-8	4.46
320×320	8.73E-5	2.85	1.39E-3	1.96	1.79E-9	4.53	3.14E-9	4.56
640×640	8.13E-6	3.42	2.20E-4	2.66	6.91E-11	4.69	1.18E-10	4.73

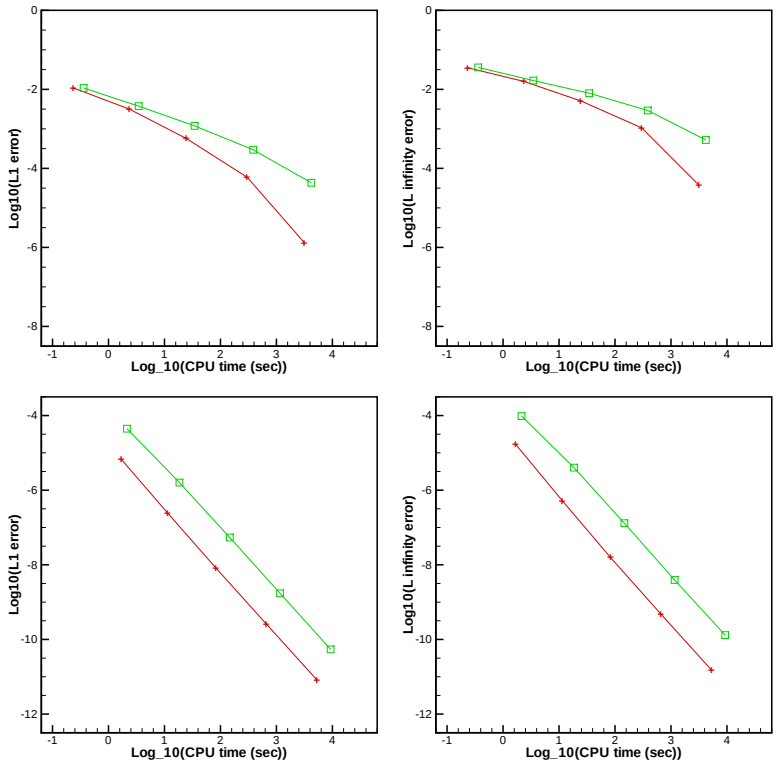

Figure 3.4: 2D-Euler equations: initial data $\rho(x, y, 0) = 1 + 0.999 \sin(x + y)$, $\mu(x, y, 0) = 1$, $\nu(x, y, 0) = 1$ and $p(x, y, 0) = 1$. Computing time and error. Plus signs and a solid line denote the results of the MWENO scheme; squares and a solid line denote the results of the WENO scheme. From top to bottom: the third order scheme; the fifth order scheme.

The zoomed in picture for different schemes and the time history of the points where the WENO reconstruction procedure is used in MWENO schemes are shown in Figure 3.5. We observe that the computational results by the MWENO schemes are better than those by the WENO schemes.

Example 3.4. A higher order scheme would show its advantage when the solution contains both shocks and complex smooth region structures. A typical example for this is the problem of shock interaction with entropy waves [18]. We solve the Euler equations (3.1) with a moving Mach=3 shock interacting with sine waves in density: $(\rho, \mu, p, \gamma)^T = (3.857143, 2.629369, 10.333333, 1.4)^T$ for $x \in [-5, -4)$; $(\rho, \mu, p, \gamma)^T = (1+0.2\sin(5x), 0, 1, 1.4)^T$ for $x \in [-4, 5]$. The computed density ρ is plotted at $T = 1.8$ against the referenced "exact" solution which is a converged solution computed by the fifth order finite difference WENO scheme [12] with 2000 grid points in Figure 3.6. The zoomed in picture for different schemes and the time history of the points where the WENO reconstruction procedure is used in MWENO scheme are also shown in Figure 3.6. We can also see that the computational results by the MWENO schemes are better than those by the WENO schemes.

Example 3.5. We now consider the interaction of two blast waves. The initial conditions are:

$$(\rho, u, p, \gamma)^T = \begin{cases} (1, 0, 10^3, 1.4)^T, & 0 < x < 0.1, \\ (1, 0, 10^{-2}, 1.4)^T, & 0.1 < x < 0.9, \\ (1, 0, 10^2, 1.4)^T, & 0.9 < x < 1. \end{cases} \tag{3.4}$$

The computed density ρ is plotted at $T = 0.038$ against the reference "exact" solution which is a converged solution computed by the fifth order finite difference WENO scheme [12] with 2000 grid points in Figure 3.7. Then the zoomed in picture for different schemes and the time history of the points where the WENO reconstruction procedure is used in MWENO scheme are shown in Figure 3.7. The MWENO schemes could get much better resolution than WENO schemes.

Example 3.6. The Sedov blast wave problem. This problem contains very low density with strong shocks. The exact solution is specified in [14, 17]. The computing domain is

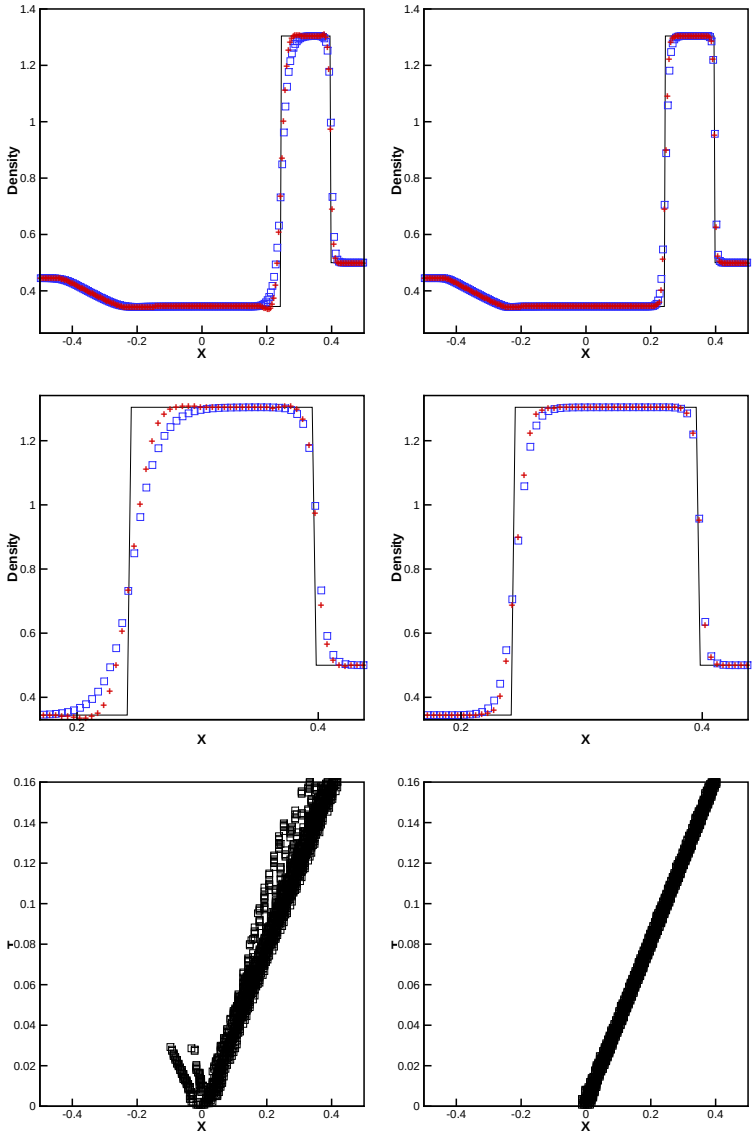

Figure 3.5: The Lax problem. T=0.16. From top to bottom: density; density zoomed in; the points where the WENO reconstruction procedure is used in MWENO scheme . Solid line: the exact solution; plus signs: the results of MWENO scheme; squares: the results of WENO scheme. From left to right: the third order scheme; the fifth order scheme. Grid points: 200.

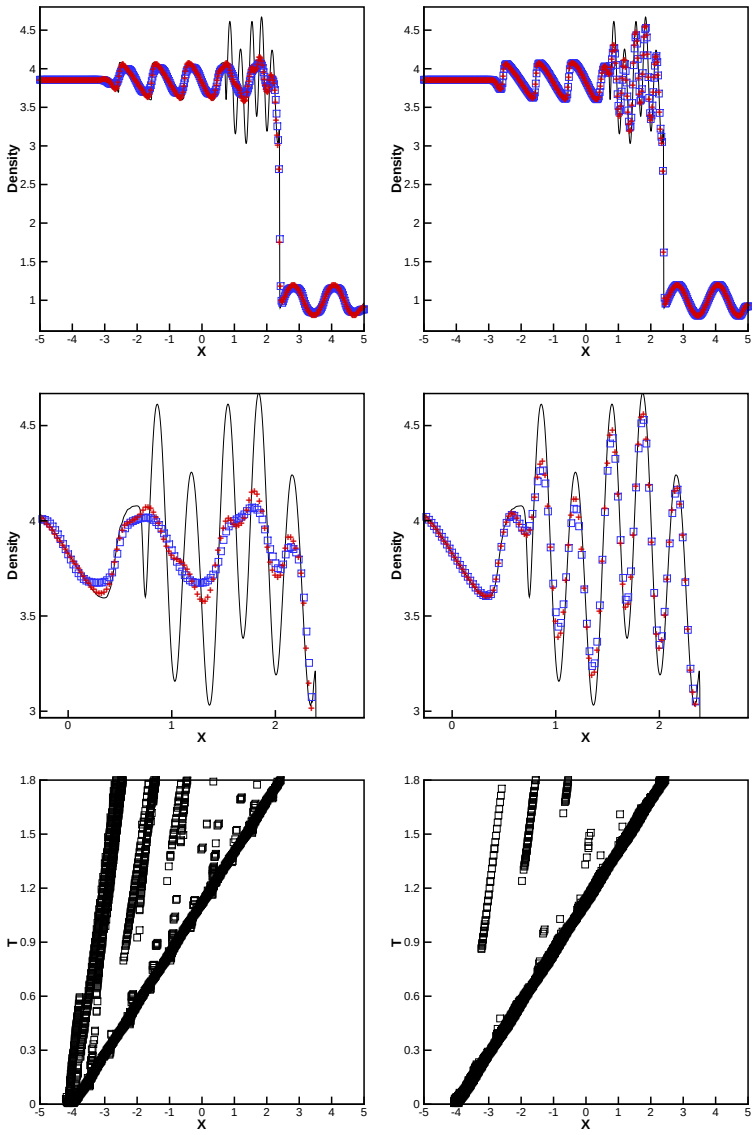

Figure 3.6: The shock density wave interaction problem. T=1.8. From top to bottom: density; density zoomed in; the points where the WENO reconstruction procedure is used in MWENO scheme . Solid line: the exact solution; plus signs: the results of MWENO scheme; squares: the results of WENO scheme. From left to right: the third order scheme; the fifth order scheme. Grid points: 400.

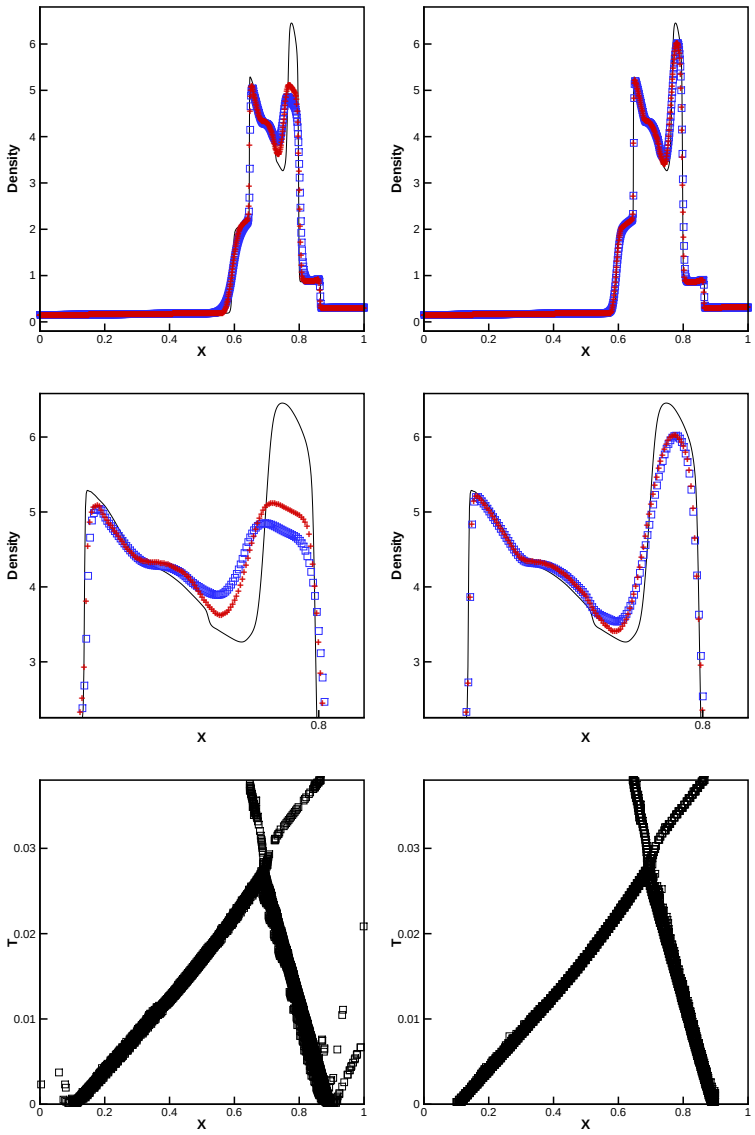

Figure 3.7: The blast wave problem. T=0.038. From top to bottom: density; density zoomed in; the points where the WENO reconstruction procedure is used in MWENO scheme. Solid line: the exact solution; plus signs: the results of MWENO scheme; squares: the results of WENO scheme. From left to right: the third order scheme; the fifth order scheme. Grid points: 800.

$[-2, 2]$ and initial conditions are: $\rho = 1$, $\mu = 0$, $E = 10^{-12}$ everywhere except that the energy in the center cell is the constant $\frac{3200000}{\Delta x}$. The final computing time is $T = 0.001$. The WENO schemes do not work for the case. The computational results by MWENO schemes including the density, velocity, pressure and the time history of the points where the WENO reconstruction procedure is used in MWENO schemes are shown in Figure 3.8, we can see that MWENO schemes work well for this extreme test case.

Example 3.7. The double rarefaction wave problem [15]. This test case has the low pressure and low density regions and is hard to be simulated precisely. The initial conditions are: $(\rho, \mu, p, \gamma)^T = (7, -1, 0.2, 1.4)^T$ for $x \in [-1, 0)$; $(\rho, \mu, p, \gamma)^T = (7, 1, 0.2, 1.4)^T$ for $x \in [0, 1]$. The final computing time is $T = 0.6$. Again, the WENO schemes do not work for the case. The computational results by MWENO including the density, velocity, pressure and the time history of the points where the WENO reconstruction procedure is used in MWENO schemes are shown in Figure 3.9, we also can see that MWENO3 and MWENO5 schemes could get good performance for this extreme one dimensional test case.

Example 3.8. The Leblanc problem [15]. The initial conditions are: $(\rho, \mu, p, \gamma)^T = (2, 0, 10^9, 1.4)^T$ for $x \in [-10, 0)$; $(\rho, \mu, p, \gamma)^T = (0.001, 0, 1, 1.4)^T$ for $x \in [0, 10]$. The final computing time is $T = 0.0001$. The computational results by MWENO schemes including the density, velocity, pressure and the time history of the points where the WENO reconstruction procedure is used in MWENO schemes are shown in Figure 3.10, again, we also can see that MWENO work well for this extreme test case and the WENO schemes break down for this case.

Example 3.9. Double Mach reflection problem. We solve the Euler equations (3.2) in a computational domain of $[0, 4] \times [0, 1]$. A reflection wall lies at the bottom of the domain starting from $x = \frac{1}{6}$, y=0, making a 60^o angle with the x-axis. The reflection boundary condition is used at the wall, which for the rest of the bottom boundary (the part from $x = 0$ to $x = \frac{1}{6}$), the exact post-shock condition is imposed. At the top boundary is the exact motion of the Mach 10 shock and $\gamma = 1.4$. The results are shown at $T = 0.2$. We

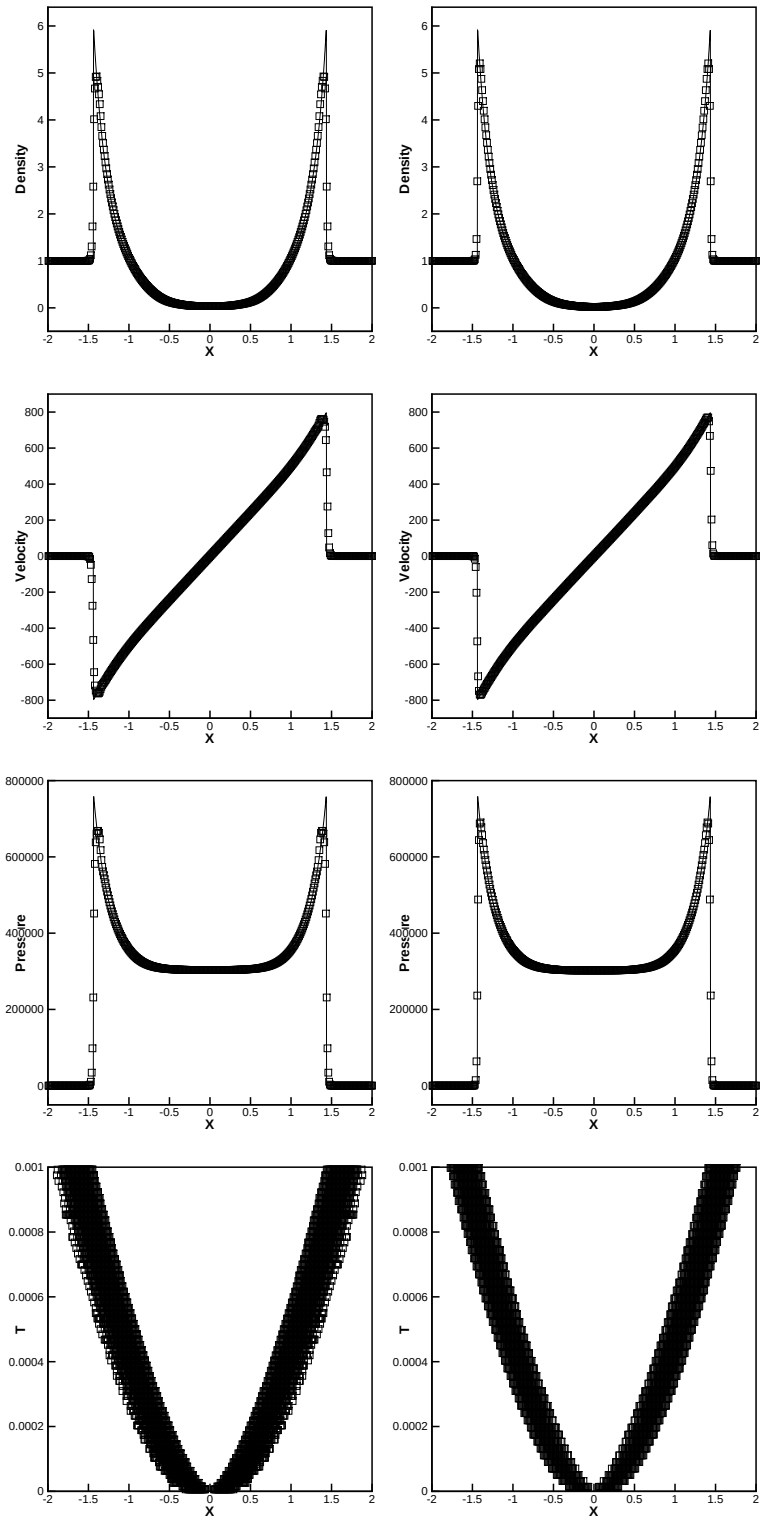

Figure 3.8: The Sedov blast wave problem. T=0.001. From top to bottom: density; velocity; pressure; the points where the WENO reconstruction procedure is used in MWENO scheme. Solid line: the exact solution; squares: the results of MWENO scheme. From left to right: MWENO3 scheme; MWENO5 scheme. Grid points: 400.

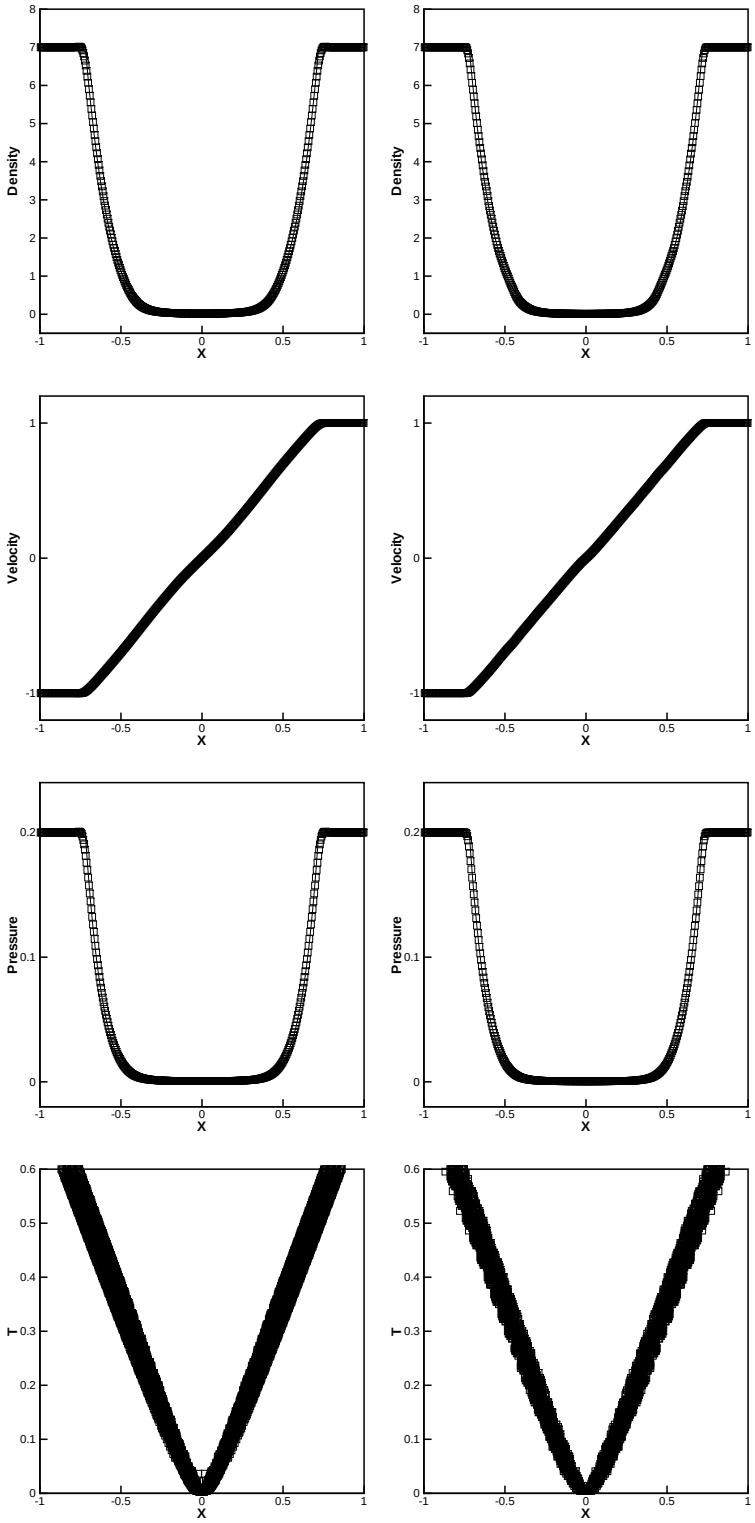

Figure 3.9: The double rarefaction wave problem. T=0.6. From top to bottom: density; velocity; pressure; the points where the WENO reconstruction procedure is used in MWENO scheme. Solid line: the exact solution; squares: the results of MWENO scheme. From left to right: MWENO3 scheme; MWENO5 scheme. Grid points: 400.

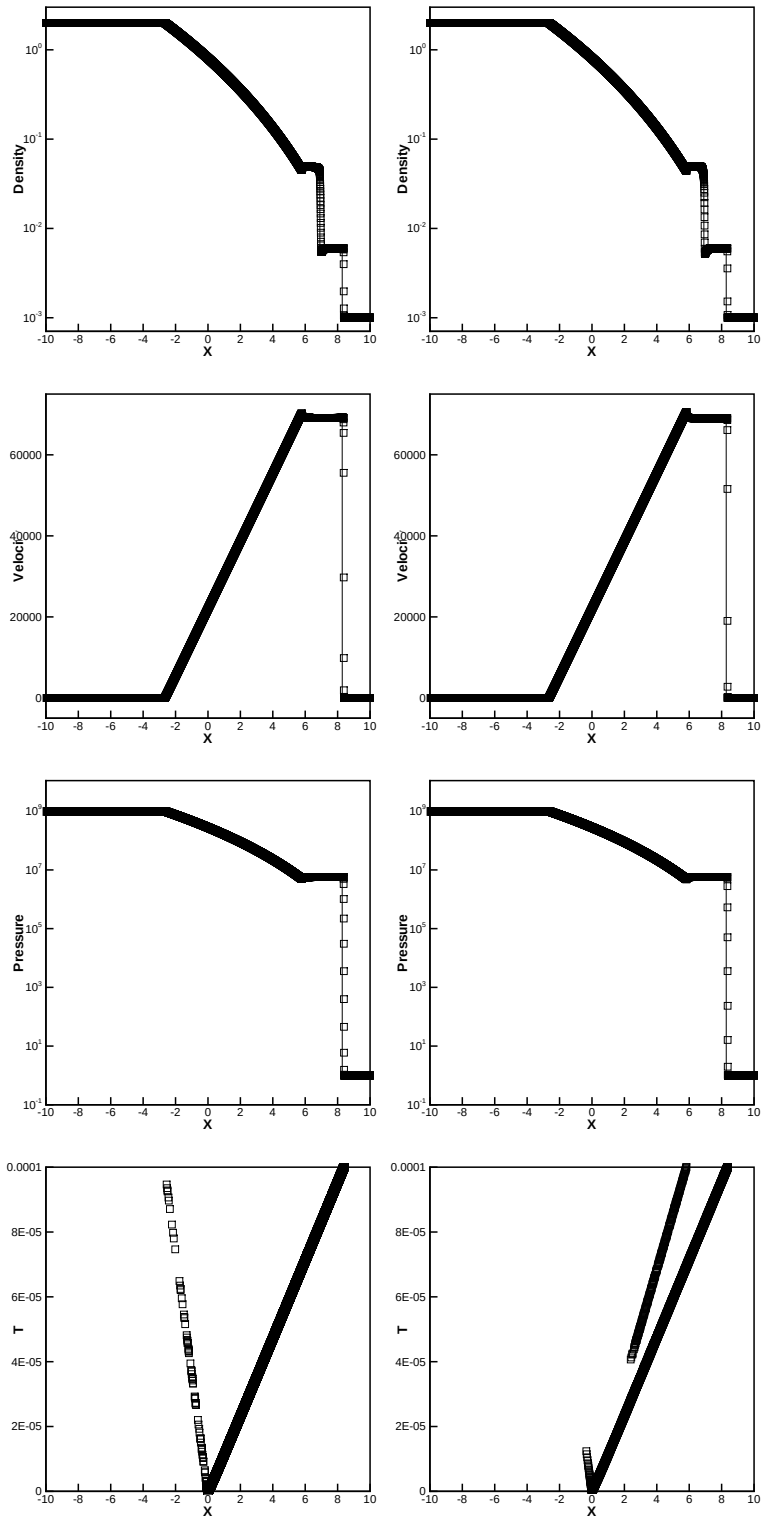

Figure 3.10: The Leblanc problem. T=0.0001. From top to bottom: log plot of density; velocity; log plot of pressure; the points where the WENO reconstruction procedure is used in MWENO scheme. Solid line: the exact solution; squares: the results of MWENO scheme. From left to right: MWENO3 scheme; MWENO5 scheme. Grid points: 6400.

present the pictures of region $[0,3]\times[0,1]$, the blow-up region around the double Mach stems and the points where the WENO reconstruction procedure is used in MWENO schemes in the final time in Figure 3.11. The MWENO3 and MWENO5 schemes could gain better density resolutions than the same order WENO schemes.

Example 3.10. The two dimensional double rarefaction wave problem [15]. The initial conditions are: $(\rho,\mu,\nu,p,\gamma)^T=(7,-1,0,0.2,1.4)^T$ for $(x,y)\in[-1,0)\times[-1,1]$; $(\rho,\mu,\nu,p,\gamma)^T=(7,1,0,0.2,1.4)^T$ for $(x,y)\in[0,1]\times[-1,1]$. The final computing time is $T=0.6$. The computational results by MWENO schemes including the density, velocity, pressure and the final time of the points where the WENO reconstruction procedure is used in MWENO schemes for the MWENO schemes are shown in Figure 3.12. We can see that MWENO schemes work well for this extreme test case, but the WENO schemes do not work for the case.

Example 3.11. The two dimensional Sedov problem [14, 17]. The initial conditions are: ρ=1, μ=0, ν=0, E=10^{-12} everywhere except that the energy in the lower left corner cell is the constant $\frac{0.244816}{\Delta x\Delta y}$ and $\gamma=1.4$. The final time is $T=1$. The computational results by MWENO schemes including the density and the final time of the points where the WENO reconstruction procedure is used in MWENO schemes are shown in Figure 3.13. Again, we can see that MWENO work well for this extreme test case, but the WENO schemes do not work for the case.

Example 3.12. The high Mach number astrophysical jet problem. For solving the gas and shocks which are discovered by using the Hubble space telescope, one can implement theoretical models in a gas dynamics simulator [4, 5, 6]. A Mach 80 problem (i.e. the Mach number of the jet inflow is Mach 25 with respect to the sound speed in the light ambient gas and Mach 80 with respect to the sound speed in the heavy jet gas) is proposed without the radiative cooling. The initial conditions are: the computational domain is [0,2] × [-0.5,0.5] and is full of the ambient gas with $(\rho,\mu,\nu,p,\gamma)^T=(0.5,0,0,0.4127,5/3)^T$. The boundary conditions for the right, top and bottom are outflow. For the left boundary $(\rho,\mu,\nu,p,\gamma)^T=(5,30,0,0.4127,5/3)^T$ for $y\in[-0.05,0.05]$ and $(\rho,\mu,\nu,p,\gamma)^T=(0.5,0,0,0.4127,5/3)^T$ oth-

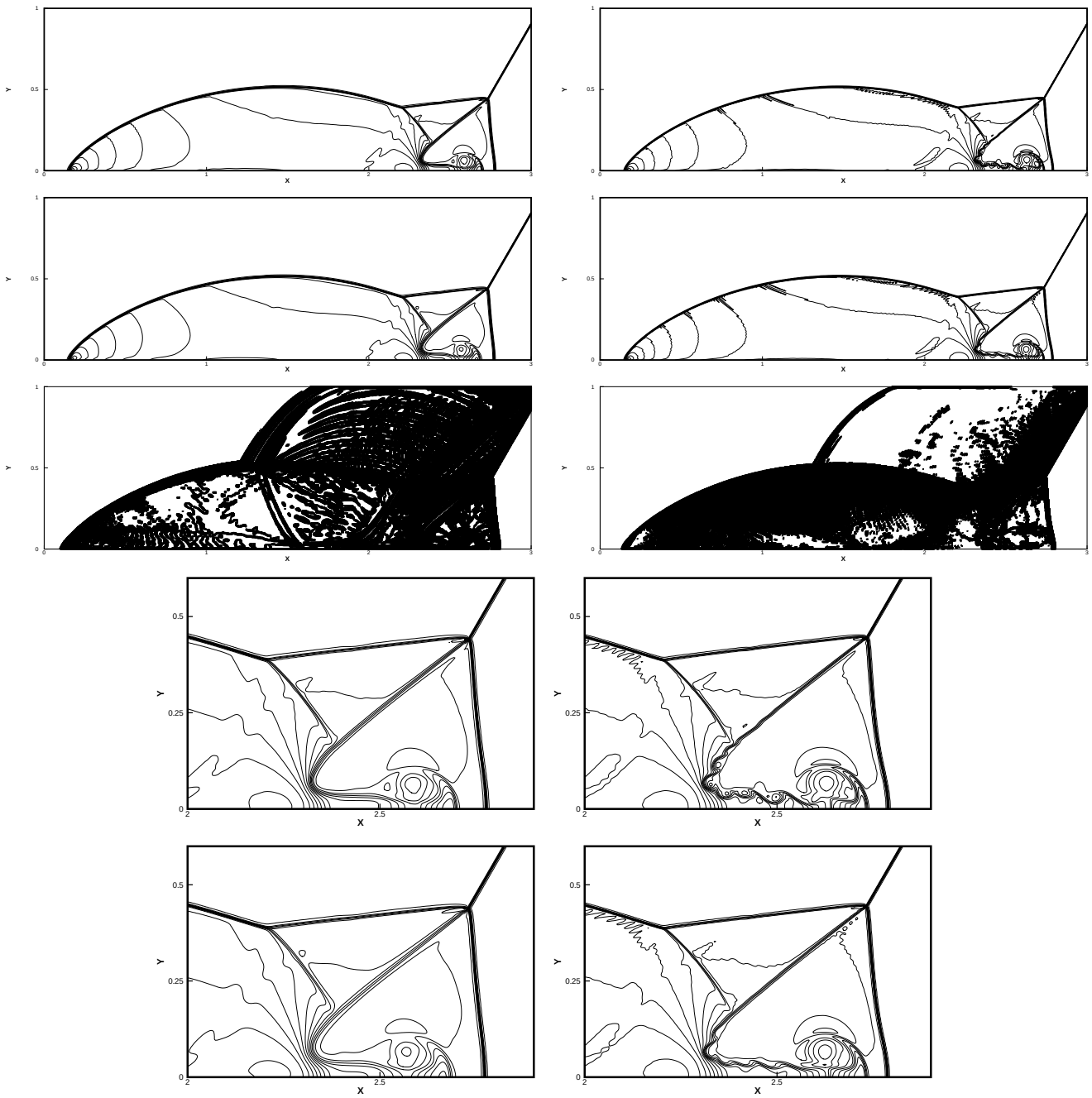

Figure 3.11: Double Mach reflection problem. T=0.2. 30 equally spaced density contours from 1.5 to 22.7. From top to bottom: MWENO scheme; WENO scheme; Squares denote the points where the WENO reconstruction procedure is used in MWENO schemes; zoomed in. From left to right: third order scheme; fifth order scheme. Grid points: 1600×400.

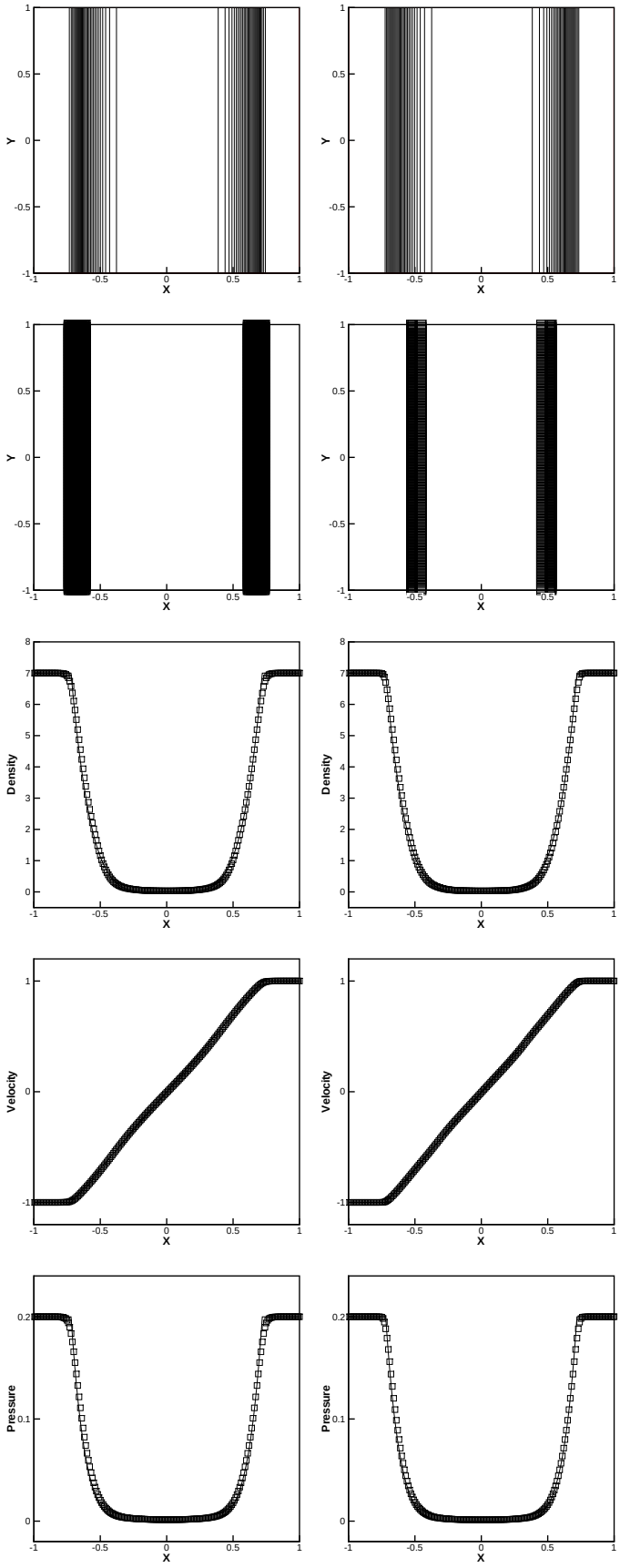

Figure 3.12: The 2D double rarefaction wave problem. T=0.6. From top to bottom: 30 equally spaced density contours from 0.25 to 6.77; the points where the WENO reconstruction procedure is used in MWENO scheme; cut at $y = 0$ for the 2D problem: density, velocity and pressure. Solid line: the exact solution; squares: the results of MWENO scheme. From

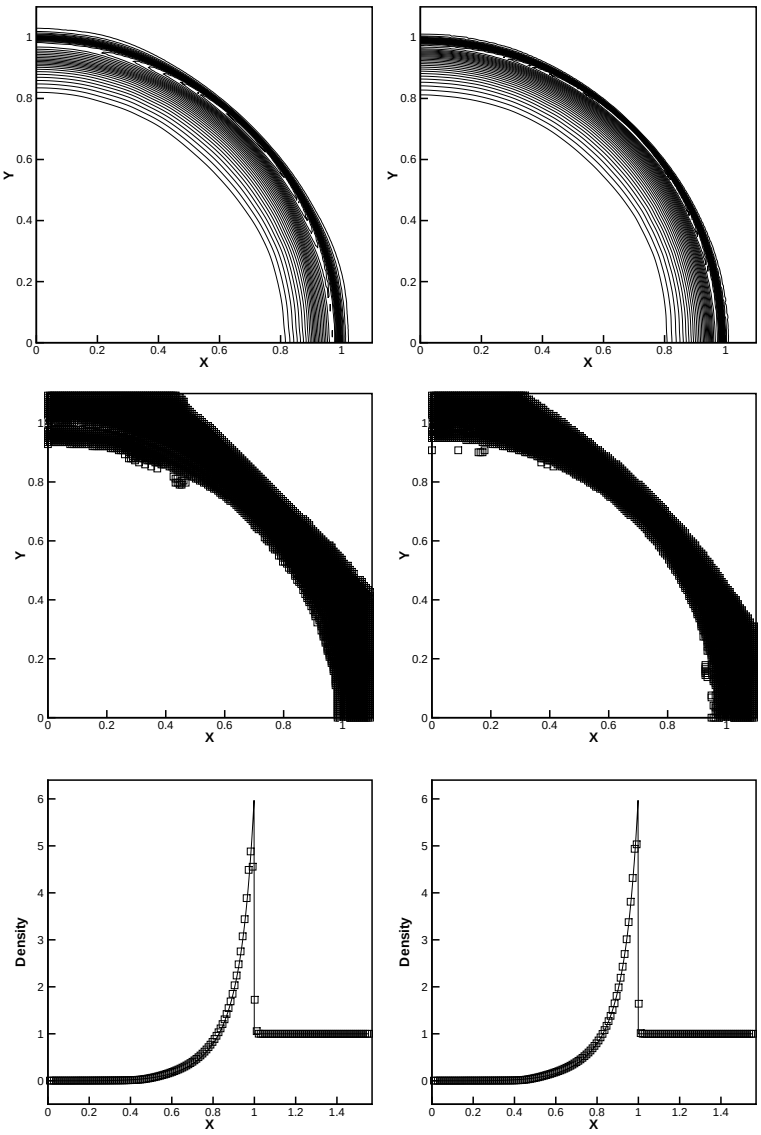

Figure 3.13: The 2D Sedov problem. T=1. From top to bottom: 30 equally spaced density contours from 0.95 to 5; the points where the WENO reconstruction procedure is used in MWENO schemes; density is projected to the radical coordinates. Solid line: the exact solution; squares: the results of MWENO scheme. From left to right: MWENO3 scheme; MWENO5 scheme. Grid points: 160×160.

erwise. The final time is $T = 0.07$. The density, pressure, temperature and the final time of the points using the WENO methodology for the MWENO3 and MWENO5 schemes are shown in Figure 3.14. Then a Mach 2000 problem (i.e. the Mach number of the jet inflow is Mach 25 with respect to the sound speed in the light ambient gas and Mach 2000 with respect to the sound speed in the heavy jet gas) is proposed without the radiative cooling again. The initial conditions are: the computational domain is [0,1] × [-0.25,0.25] and is full of the ambient gas with $(\rho, \mu, \nu, p, \gamma)^T = (0.5, 0, 0, 0.4127, 5/3)^T$. The boundary conditions for the right, top and bottom are outflow. For the left boundary $(\rho, \mu, \nu, p, \gamma)^T = (5, 800, 0, 0.4127, 5/3)^T$ for $y \in [-0.05, 0.05]$ and $(\rho, \mu, \nu, p, \gamma)^T = (0.5, 0, 0, 0.4127, 5/3)^T$ otherwise. The final time is t=0.001. The density, pressure, temperature and the final time of the points where the WENO reconstruction procedure is used in MWENO schemes are shown in Figure 3.15. Again, we can see that MWENO work well for this extreme test case, but the WENO schemes do not work for the case.

4 Concluding remarks

In this paper, a new type of high order accurate finite difference MWENO schemes are constructed for solving the hyperbolic conservation laws. Comparing them with the WENO schemes [12, 18], the new MWENO schemes are more efficient and robust, and can be applied to compute rather extreme test cases such as the Sedov blast wave, the Leblanc and the high Mach number astrophysical jet problems et al. by using a normal CFL number without any further positivity preserving procedure for the purpose of controlling the appearance of the negative density and pressure. Extensive numerical tests including the Sedov blast wave, the Leblanc and the high Mach number astrophysical jet problems et al. are provided to illustrate the good performance of the MWENO schemes.

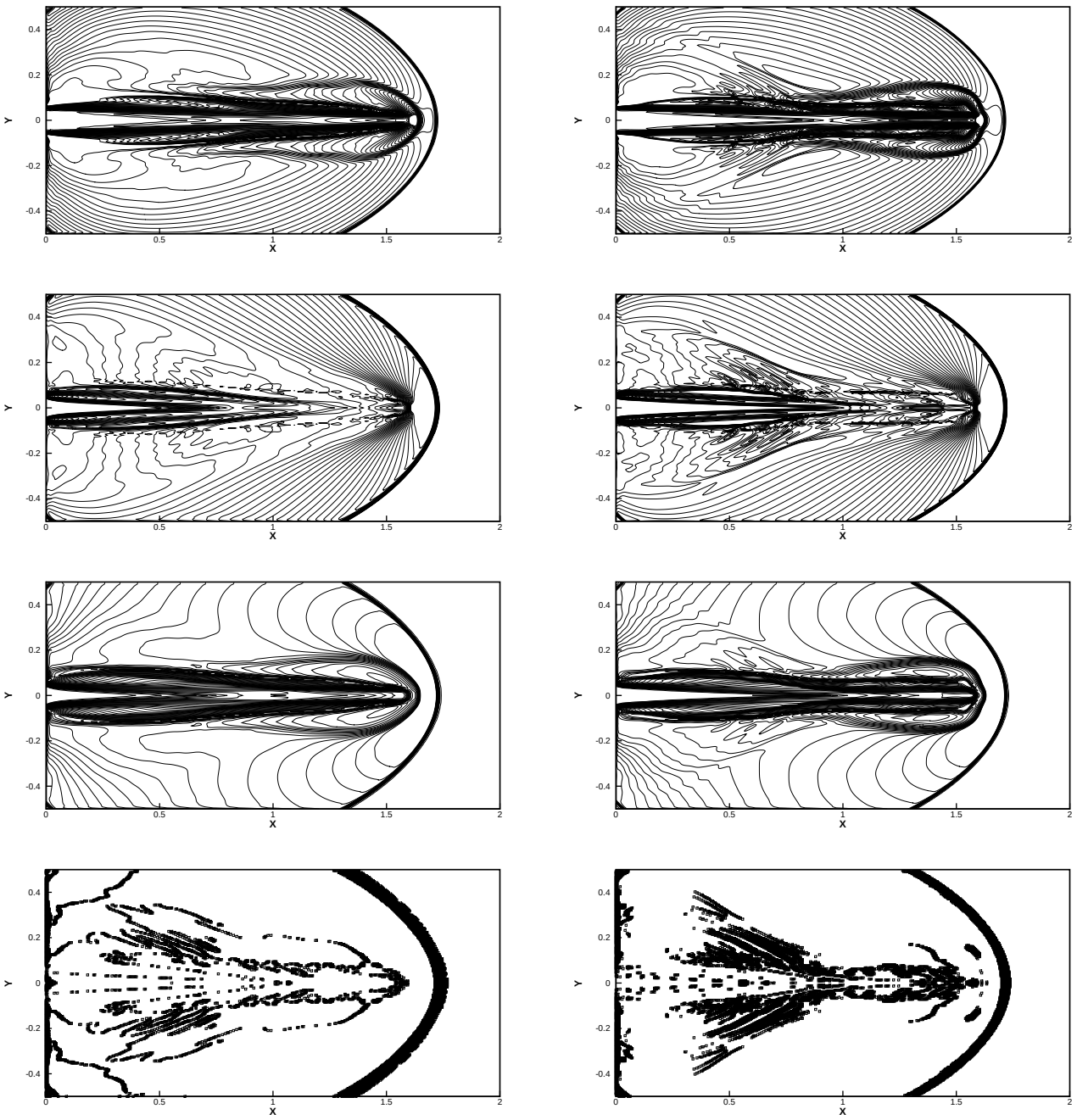

Figure 3.14: Simulation of Mach 80 jet without radiative cooling problem. T=0.07. Scales are logarithmic. From top to bottom: 40 equally spaced density contours from -2 to 3; 40 equally spaced pressure contours from -0.5 to 5; 40 equally spaced temperature contours from -2 to 4.5; the points where the WENO reconstruction procedure is used in MWENO schemes. From left to right: MWENO3 scheme; MWENO5 scheme. Grid points: 448×224.

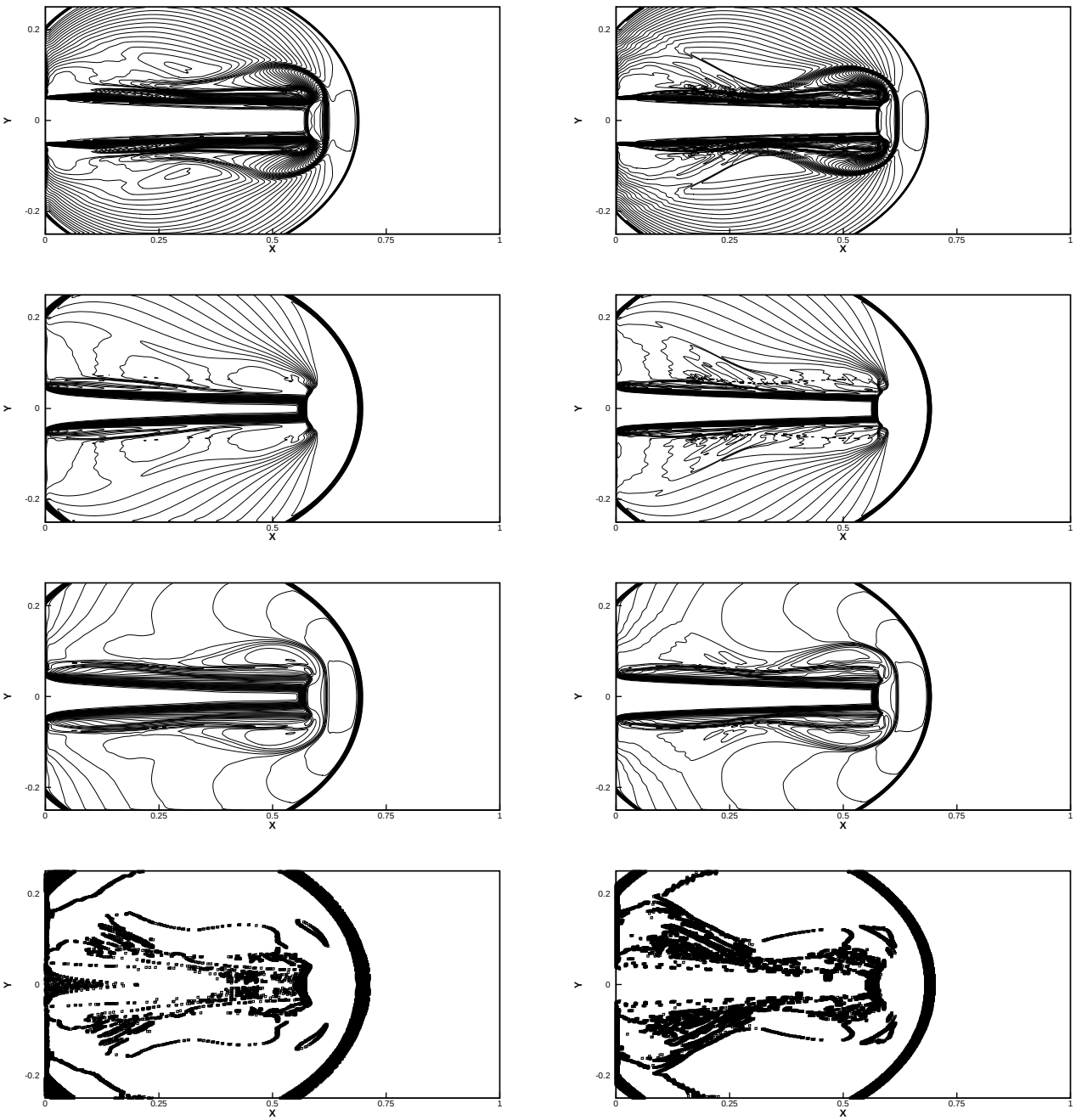

Figure 3.15: Simulation of Mach 2000 jet without radiative cooling problem. T=0.001. Scales are logarithmic. From top to bottom: 40 equally spaced density contours from -2 to 3; 40 equally spaced pressure contours from -2 to 11; 40 equally spaced temperature contours from -3 to 12.5; the points where the WENO reconstruction procedure is used in MWENO schemes. From left to right: MWENO3 scheme; MWENO5 scheme. Grid points: 640×320.

References

[1] J. Casper, Finite-volume implementation of high-order essentially nonoscillatory schemes in two dimensions, AIAA Journal, 30 (1992), 2829-2835.

[2] J. Casper and H.L. Atkins, A finite-volume high-order ENO scheme for two-dimensional hyperbolic systems, J. Comput. Phys., 106 (1993), 62-76.

[3] S.J. Fan, A new extracting formula and a new distinguishing means on the one variable cubic equation, Journal of Hainan Normal University (Natural Science Edition), 2 (2) (1989), 91-98. (in chinese).

[4] C. Gardner and S. Dwyer, Numerical simulation of the XZ Tauri supersonic astrophysical jet, Acta Mathemacita Scientia, 29 (2009), 1677-1683.

[5] Y. Ha and C. Gardner, Positive scheme numerical simulation of high Mach number astrophysical jets, J. Sci. Comput., 34 (2008), 247-259.

[6] Y. Ha, C. Gardner, A. Gelb and C.-W. Shu, Numerical simulation of high Mach number astrophysical jets with radiative cooling, J. Sci. Comput., 24 (2005), 597-612.

[7] A. Harten, High resolution schemes for hyperbolic conservation laws, J. Comput. Phys., 49 (1983), 357-393.

[8] A. Harten, Preliminary results on the extension of ENO schemes to two-dimensional problems, in Proceedings, International Conference on Nonlinear Hyperbolic Problems, Saint-Etienne, 1986, Lecture Notes in Mathematics, edited by C. Carasso *et al.* (Springer-Verlag, Berlin, 1987).

[9] A. Harten, B. Engquist, S. Osher and S. Chakravarthy, Uniformly high order accurate essentially non-oscillatory schemes III, J. Comput. Phys., 71 (1987), 231-323.

[10] A. Harten, and S. Osher, Uniformly high-order accurate non-oscillatory schemes, IMRC Technical Summary Rept. 2823, Univ. of Wisconsin, Madison, WI, May 1985.

[11] C. Hu and C.-W. Shu, Weighted essentially non-oscillatory schemes on triangular meshes, J. Comput. Phys., 150 (1999), 97-127.

[12] G.-S. Jiang and C.-W. Shu, Efficient implementation of weighted ENO schemes, J. Comput. Phys., 126 (1996), 202-228.

[13] Y. Jiang, Z. Xu, Parameterized maximum principle preserving limiter for finite difference WENO schemes solving convection-dominated diffusion equations. SIAM J. Sci. Comput., 35 (2013), 2524-2553.

[14] V.P. Korobeinikov, Problems of Point-Blast Theory, American Institute of Physics, 1991.

[15] T. Linde, P.L. Roe, Robust Euler codes, in: 13th Computational Fluid Dynamics Conference, AIAA Paper-97-2098.

[16] X.D. Liu, S. Osher and T. Chan, Weighted essentially non-oscillatory schemes, J. Comput. Phys., 115 (1994), 200-212.

[17] L.I. Sedov, Similarity and Dimensional Methods in Mechanics, Academic Press, New York, 1959.

[18] C.-W. Shu, High order weighted essentially nonoscillatory schemes for convection dominated problems, SIAM Review, 51 (2009), 82-126.

[19] C.-W. Shu and S. Osher, Efficient implementation of essentially non-oscillatory shock capturing schemes, J. Comput. Phys., 77 (1988), 439-471.

[20] C.-W. Shu and S. Osher, Efficient implementation of essentially non-oscillatory shock capturing schemes, II, J. Comput. Phys., 83 (1989), 32-78.

[21] T. Xiong, J.-M. Qiu and Z. Xu, Parametrized positive preserving flux limiters for the high order finite difference WENO scheme solving compressible Euler equations, J. Sci. Comput., in press.

[22] X. Zhang and C.-W. Shu, On maximum-principle-satisfying high order schemes for scalar conservation laws , J. Comput. Phys., 229 (2010), 3091-3120.

[23] X. Zhang and C.-W. Shu, On positivity preserving high order discontinuous Galerkin schemes for compressible Euler equations on rectangular meshes, J. Comput. Phys., 229 (2010), 8918-8934.

[24] X. Zhang and C.-W. Shu, Maximum-principle-satisfying and positivity-preserving high order schemes for conservation laws: Survey and new developments, Proc. the Royal Society A, 467 (2011), 2752-2776.

[25] X. Zhang and C.-W. Shu, Positivity-preserving high order finite difference WENO schemes for compressible Euler equations, J. Comput. Phys., 231 (2012), 2245-2258.

[26] Y.T. Zhang and C.-W. Shu, Third order WENO scheme on three dimensional tetrahedral meshes, Commun. Comput. Phys., 5 (2009), 836-848.